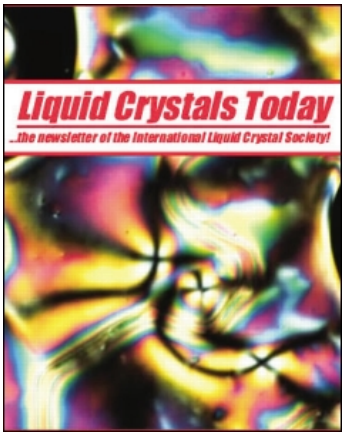

Liquid Crystals Today
Publication details, including instructions for authors and subscription information:
http://www.informaworld.com/smpp/title~content=t713681230

Polarization-analysed resonant X-ray scattering study of chiral smectic-C variant phases in freely-suspended liquid-crystal films

Peter Mach

Online publication date: 11 November 2010

To cite this Article Mach, Peter(2002) 'Polarization-analysed resonant X-ray scattering study of chiral smectic-C variant phases in freely-suspended liquid-crystal films', Liquid Crystals Today, 11: 1, 1 — 5
To link to this Article: DOI: 10.1080/135831402010127750
URL: http://dx.doi.org/10.1080/135831402010127750

Taylor & Francis
Taylor & Francis Group

Polarization-analysed resonant X-ray scattering study of chiral smectic-C variant phases in freely-suspended liquid-crystal films

PETER MACH
Bell Laboratories, Lucent Technologies, Murray Hill, NJ 07974, USA

1. Introduction

Inspired by the discovery in 1989 [1] of the antiferroelectric chiral smectic C (SmC^*_A) phase in the MHPOBC compound, studies during the past decade on many newly synthesized liquid-crystal materials led to the identification of other SmC* variants, including, besides the previously known ferroelectric SmC*, the so-called SmC^*_α and also the *ferri*electric phases SmC^*_{FI1} and SmC^*_{FI2}. A complete series of such phases, in order of decreasing temperature, could typically appear as SmC^*_α, SmC*, SmC^*_{FI2}, SmC^*_{FI1}, and SmC^*_A [2]. A proper understanding of the mechanisms giving rise to such a rich sequence of antiferro- and ferri-electric ordering is of fundamental interest to condensed matter researchers. This is particularly true since the molecules in these phases lack the truly long-range positional order typically expected for structures that involve contributions from antiferroelectric interactions. At the same time, a detailed picture of the molecular arrangements characterizing the SmC* variants is also of technological importance, since several phases, most notably SmC* and SmC^*_A, have already been exploited in electro-optic devices for their rapid bistable or tristable switching behaviour.

Numerous experimental probes were applied in the past to characterize the physical properties of the SmC* variants; published reports included electro-optic [3, 4], conoscopy [3, 5], optical [6], ellipsometric [7], and X-ray [8] studies. Unfortunately, these methods were generally unable to give direct pictures of the relevant molecular orderings, even in the case of conventional X-ray scattering, normally a very powerful structural tool. Our research group chose to apply the technique of resonant X-ray scattering in order to overcome this difficulty, and to obtain detailed information about the intriguing differences between the ferro-, ferri-, and anti-ferroelectric liquid-crystal structures. The collected resonant X-ray data revealed distinct structural periodicities associated with the various chiral SmC phases, as exhibited by one thiobenzoate liquid-crystal enantiomer compound (10OTBBB1M7) and the SmC_A phase of its racemic counterpart. Our results showed the existence of two-, three-, and four-layer superlattice periods in the SmC^*_A, SmC^*_{FI1}, and SmC^*_{FI2} phases, respectively, along with periodicity incommensurate with layer spacing in SmC^*_α. The experimental technique developed includes polarization analysis on the X-rays contributing to each of the resonant diffraction peaks associated with the superlattices of the chiral SmC variants. Calculations of the tensorial structure factors appropriate for resonant X-ray scattering [9, 10] provided distinct predictions for how diffracted X-ray polarization states should differ depending on the model used to describe the molecular structures. By making comparisons of the polarization-analysed resonant X-ray data collected from 10OTBBB1M7 against the predictions of several proposed molecular arrangements, it was possible to show that only a previously-proposed 'clock' model [11] could consistently describe the resonant X-ray peaks observed in all the variant SmC* phases.

2. Structure of SmC* phases studied, and sample geometry

In the smectic phases, liquid-crystal molecules organize to give a layered centre-of-mass distribution. Within any given layer, the positional order is purely liquid-like, but the molecules have their long axes strongly oriented along a director, **n**. The director is either along the layer normal **z** (SmA phase), or is inclined with respect to the layer normal by some tilt angle θ (SmC phases). Within the SmC phases, a projection (**c**) of the molecular director **n** onto the xy layer plane can be considered. The angle between **c** and the x-axis in the j^{th} layer is denoted as Ψ_j, and the change in Ψ_j between adjacent layers j and $(j+1)$ as $\Delta\Psi_j$; a schematic picture of this situation is given in figure 1. If the liquid crystal molecules are chiral, an overall helical rotation of **c** develops with a pitch, P_o, $\sim 1\,\mu m$. It is in the detailed progression of Ψ_j and $\Delta\Psi_j$ from layer to layer where proposed models of the molecular arrangements of the SmC* variants differ.

For the resonant scattering X-ray work, the liquid crystal compounds were studied in the form of thick, free-standing films, with the X-rays incident in a Bragg geometry. In contrast to typical bulk sample cell preparations, a free-standing film provides a well-defined, uniform orientation of the smectic layers without requiring any extra aligning surface that would attenuate the X-ray intensity.

Liquid Crystals Today ISSN 1464-5181 online © 2002 Taylor & Francis Ltd
http://www.tandf.co.uk/journals
DOI: 10.1080/13583140201012775O

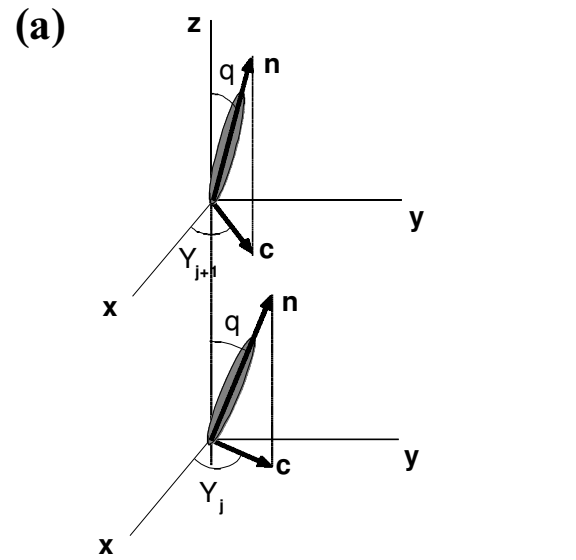

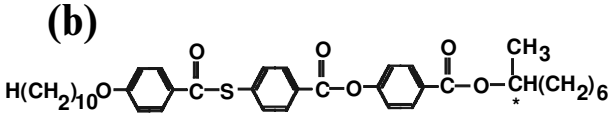

Figure 1. (a) Schematic diagram illustrating the orientation of molecules in neighbouring SmC* layers. The tilt angle θ in layers j and $(j+1)$ is the same, while azimuthal angles Ψj and $\Psi j+1$ differ. **z**, **n**, and **c** are coplanar. (b) The molecular structure of 10OTBBB1M7, including the sulphur atom with K absorption edge at 2475 eV.

The primary material studied in the original polarized X-ray scattering experiment was 10OTBBB1M7, whose molecular structure is also given in figure 1. The bulk 10OTBBB1M7 enantiomer shows the following phase sequence: Isotropic (153°C) SmA (124°C) SmC^*_α (120°C) SmC* (119°C) SmC^*_{FI2} (114°C) SmC^*_{FI1} (112°C) SmC^*_A (110°C) crystal. A critical feature of 10OTBBB1M7 for the purposes of the experiment is the sulphur atom contained within the centre portion of the molecule. Conventional X-ray diffraction along the Q_z reciprocal space direction probes the in-plane-averaged electron density. All of the SmC* variants give Q_z peaks only at integral multiples of $Q_o = 2\pi/d$, where d is the smectic layer spacing. Therefore, the z-projected electron density is identical for all of the variants, and they differ from one another only by symmetry elements such as glide planes or screw axes along **z**. By working with x-rays whose energy is at the sulphur's K absorption edge, the structure factor becomes a tensor instead of the conventional scalar [9, 10]. The scattered x-ray intensity now varies depending on the molecular orientation, since the off-diagonal tensor components depend on the orientation of the bonds around the sulphur atom with respect to the polarization of the incident X-ray beam. Because $\Delta\Psi_j$ arrangements of various SmC* subphases are distinct, under this circumstance the resonant X-ray diffraction is capable of revealing the structural differences.

3. Experimental description

The original resonant scattering X-ray studies were performed at beamline X-19A of the National Synchrotron Light Source (NSLS) at Brookhaven National Laboratory. The central component of the overall apparatus was a heated sample chamber; the liquid crystals, spread inside as approx. 1-cm diameter freely-suspended films, could thus be held at appropriate elevated temperatures. A visual estimation of film thickness, as well as an independent monitor of the optical textures distinguishing the various phases, was provided by microscope/CCD camera observation under polarized light. The X-ray elements also included an assembly upstream of the sample chamber which allowed retractable insertion of bulk powder sample into the X-ray beam, with emitted fluorescent intensity collected as a function of incident X-ray energy. This allowed us to precisely determine the appropriate sulphur resonant K edge (2475 eV) for the materials studied [12].

The downstream side of the X-ray flight path incorporated the polarimeter assembly. Rotating a pyrolytic graphite crystal about the so-called χ_a axis, defined by the direction of the beam incident on this crystal, while at the same time keeping the incidence angle, θ_a, fixed to the Bragg angle, modulates the intensity diffracted from the crystal in a manner depending on the incident X-rays' polarization. In the ideal case of a 45° Bragg angle, X-rays polarized linearly perpendicular to the crystal's diffraction plane will be completely diffracted, while those polarized within the diffraction plane will not diffract at all. With a Bragg angle of 48.3° at 2.475 KeV, pyrolytic graphite provided excellent polarization discrimination for our measurements. In practice, when analysed by our polarimeter assembly, linearly σ-polarized x-rays (σ defined here as a unit vector in the plane of the synchrotron ring) give a characteristic $\sin^2(\chi_a)$ profile 90 degrees offset in χ_a coordinate from the π-polarized case. This ability to distinguish σ versus π polarization was a critical feature of our experiment. For example, the tensorial structure factor calculations carried out based upon the undistorted clock model for the SmC* variants [10] specifically predicted diffraction of incident σ into outgoing π polarization for certain orders of satellite reflections from the structural superlattices. The combination of highly σ-polarized incident X-ray radiation available at the synchrotron beamline, together with diffracted X-ray polarization analysis, enabled us to conclusively test the model's predictions.

To complete the description of the experimental design, it should be noted that all components of our experiment were connected into a sealed flight path separated from beamline vacuum by an 8-μm beryllium window. During the measurements, the flight path was kept flushed with helium gas in order to avoid the prohibitive reduction in X-ray intensity which would otherwise result from air absorption at such a low X-ray energy. The film oven, and all of the components comprising the 'detection arm' of the assembly, were mounted on the theta and two-theta circles, respectively, of a Huber two-circle goniometer. An overall schematic view of our set-up, including the X-ray polarization analysis, is given in figure 2.

4. Data and discussion

Figure 3 gives a composite plot of the resonant scattering features observed in the SmC* variant phases of the 10OTBBB1M7 material [13]. The peaks at non-integer Q_z/Q_o indicate the presence of superlattices in the molecular Ψ_j and $\Delta\Psi_j$ progressions. Half-order peaks in the SmC^*_A and SmC_A phases indicate a two-layer superlattice, although the superimposed, approx. 0.5 μm optical pitch in the chiral case leads to a discernible splitting of the resonant half-order features. The one-third and one-quarter order peaks indicate three- and four-layer superlattices in SmC^*_{F11} and SmC^*_{F12}, respectively. The SmC^*_α phase is characterized by a superlattice of incommensurate pitch, which varied between 5 and 8 layers with increasing temperature within the SmC^*_α phase window. In all cases, the superlattice signature peaks disappear when the scans are repeated at X-ray energies off of resonance by more then 20 eV, leaving only the conventional first and second order layer spacing features at $Q_z = Q_o$ and $2Q_o$.

These features are well-interpreted in the context of calculations by Levelut and Pansu [10], who found that a helical structure of pitch = νd leads to resonant satellite peaks at

$$Q_z/Q_o = \ell + m[(1/\nu) + \varepsilon],$$

where $\varepsilon = d/P_o$; $\ell = 0, 1, 2, \ldots$; and $m = -2, -1, 0, 1, 2$, where the five independent m values are a consequence of the five independent tensor components in the scattering factor. The corresponding (ℓ,m) assignments to the superlattice peaks have been indicated in figure 3.

Levelut and Pansu showed that intriguing polarization effects should be seen for X-rays diffracted from such superlattice structures, depending on the specific model used for the Ψ_j and $\Delta\Psi_j$ progressions. For example, previously proposed 'Ising-like' models [14] restricted Ψ_j to a plane, and therefore $\Delta\Psi_j$ to only values of 0 or π. On the other hand, the so-called 'clock' model does not place restrictions on Ψ_j, and in an undistorted

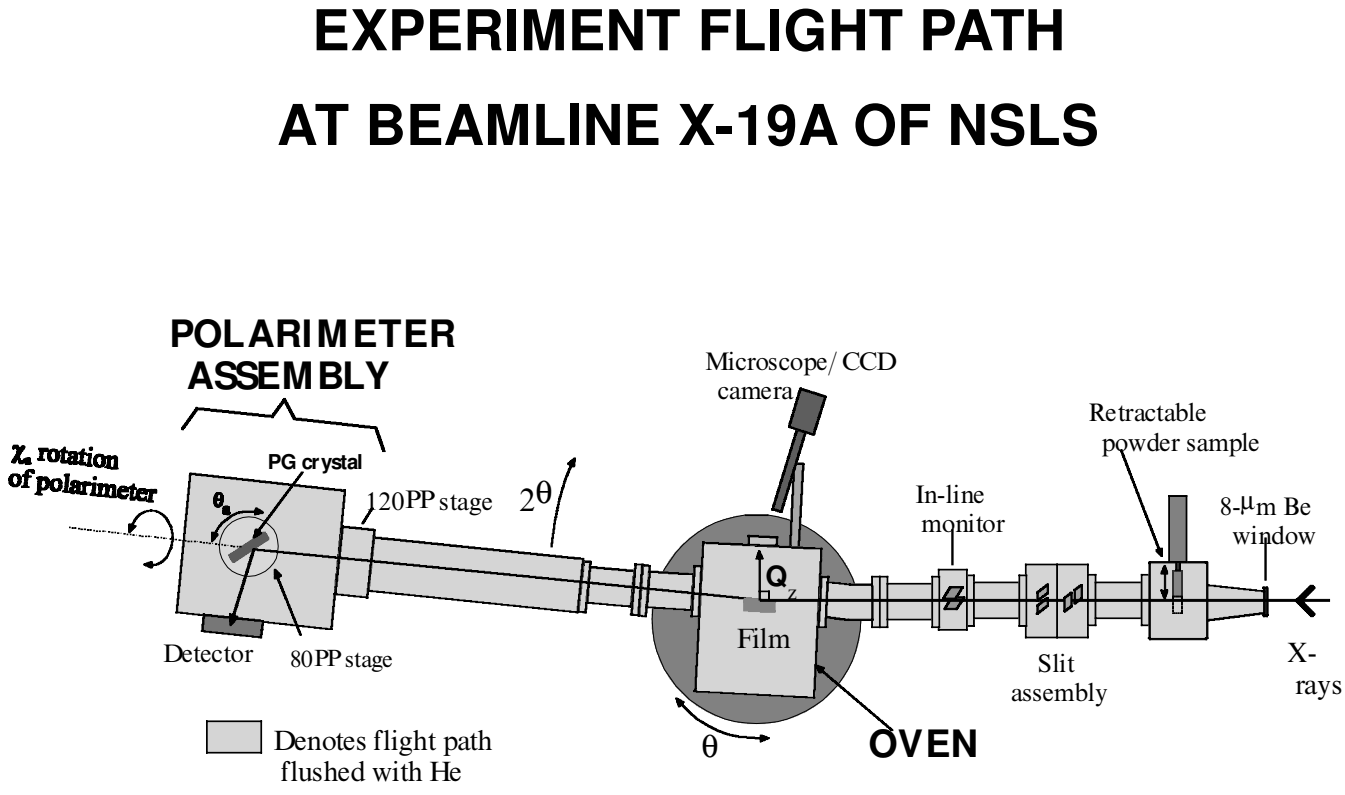

Figure 2. Schematic diagram of components in the polarized resonant X-ray scattering experiment.

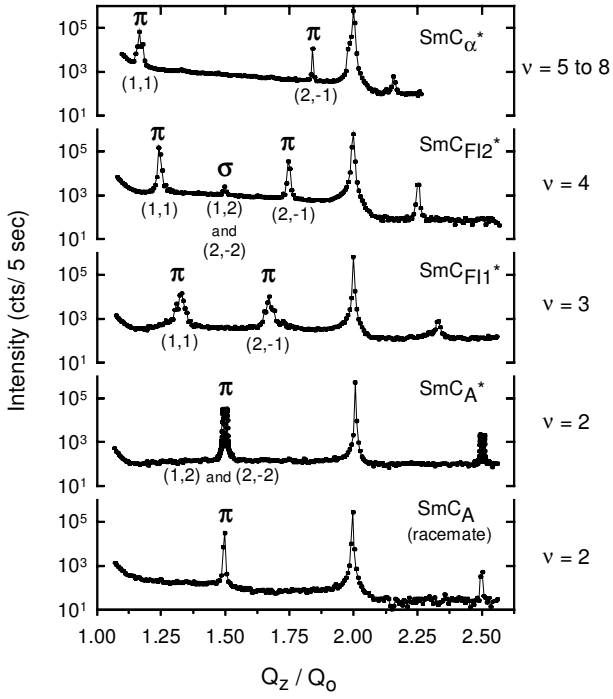

Figure 3. Composite plot of X-ray data for the SmC* variant phases observed in freely-suspended films of 10OTBBB1M7. Indicated on the plots are the deduced superlattice periods ν corresponding to each of the phases, the subsequently determined peak polarization states, and also the resonant peak satellite indices (ℓ,m) in the context of the clock model.

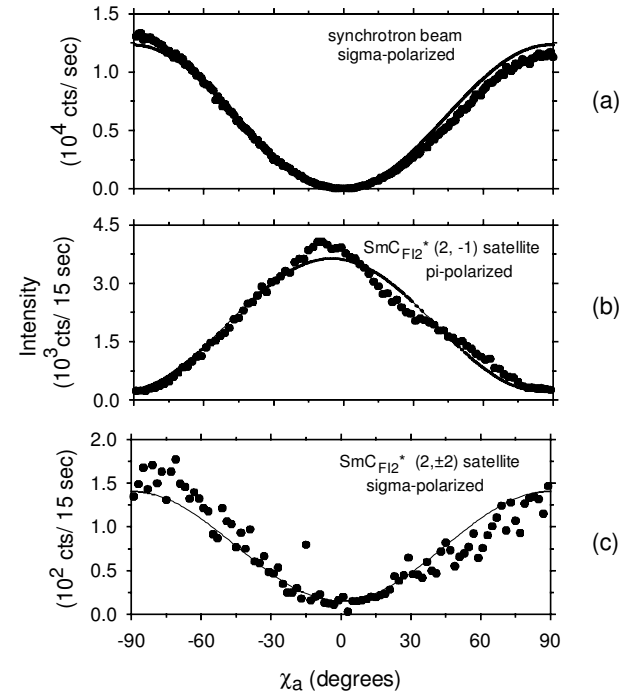

Figure 4. Composite plot of X-ray intensity collected as function of polarimeter analyser crystal angle χ^a. Plot (a) shows characteristic $\sin^2(\chi^a)$ shape for the σ-polarized direct beam-line X-rays. Plot (b) gives data for the π-polarized $m=-1$ resonant satellite peak ($Q_z/Q_o = 1.75$) in the SmC^*_{FI2} phase of 10OTBBB1M7. Plot (c) indicates σ-polarization of the $m=2$ resonant satellite ($Q_z/Q_o = 1.5$) in 10OTBBB1M7's SmC^*_{FI2} phase.

case predicts a $\Delta\Psi_j = 2\pi/\nu$. One very powerful case for discriminating between the proposed models occurs with the satellite peaks of the SmC^*_{FI2} ($\nu = 4$) phase. Two varieties of Ising-like models, so-called E-Ising and T-Ising [2, 14], had been proposed to account for the SmC* variant progressions under changing external electric field or temperature, respectively. While each yielding different $\Delta\Psi_j$ progressions for $\nu = 4$, both models predicted π-polarized $m = \pm 1$ resonant peaks from σ-polarized incident X-rays; however, the satellite feature at $m = \pm 2$ for T-Ising should be non-resonant, and therefore remain present even for X-ray energy tuned away from 2475 eV. The resonant nature of the $m = \pm 2$ feature we observed contradicted this prediction. Furthermore, under the E-Ising model, the $m = \pm 2$ resonant peaks should also be π-polarized. In a clock model, the $m = \pm 2$ peaks should preserve σ polarization. Figure 4 shows that our measurements on the $m = \pm 2$ resonant feature of SmC^*_{FI2} are consistent with a clock model, and therefore ruled out perfect Ising-like models as a description of the complete SmC* variant series [15]. The characteristic $\sin^2(\chi^a)$ profile of the incident σ-polarized beam is also given in Fig. 4, to provide a reference for the adopted coordinate system.

5. Recent developments in SmC* variant research

This article has summarized the experimental technique and data originally collected in a 1999 University of Minnesota PhD dissertation, and subsequently recognized with the Glenn H. Brown Award at the 2000 International Liquid Crystal Conference held in Sendai, Japan. The resonant scattering work provided the first direct structural evidence for superlattice periodicities characterizing a full sequence of antiferro-, ferri-, and ferroelectric chiral SmC phases. In fact, polarization-analysed resonant X-ray scattering should prove to be a powerful, general tool for revealing orientational structure features that are otherwise undetectable in soft condensed matter by conventional methods. The resonant scattering technique gives us the ability to resolve orientational order periodicities from the molecular layer to optical pitch length scales, or in other words, from angstroms to microns.

Within the past 2 years, much additional progress has been made in obtaining further information about the chiral SmC* variant phases and their molecular arrangements. For example, the evolution of incommensurate superlattice periodicity, from between 5 to 8 molecular layers, as a function of temperature within the SmC^*_α

phase of 10OTBBB1M7, as revealed by our original resonant scattering work, contradicted the previously proposed 'Devil's staircase' model for this structure, which was based on the Ising model framework. In such a staircase sequence, a series of transitions between varying, but commensurate superlattice periodicity, could be expected within the SmC^*_α phase. Since the time of the original resonant scattering results, new high-resolution ellipsometry measurements have been conducted on free-standing liquid-crystal films, corroborating a steadily evolving, incommensurate superlattice within SmC^*_α [16]. On the other hand, a number of earlier studies had detected finite biaxiality in the so-called ferrielectric phases, such as SmC^*_{FI1} and SmC^*_{FI2}. As a consequence of such measurements, a critical need arose to look for evidence of distortions in the perfect clock structure, and whether such distortions could be consistent with the resonant scattering X-ray data. In fact, both helical pitch and optical rotary power measurements [17], as well as ellipsometric studies on free-standing films [18], have since provided conclusive evidence of distortions from perfect clock arrangements in the SmC^*_{FI1} and SmC^*_{FI2} phases. Motivated by these results, a new series of resonant scattering measurements have revealed splitting of resonant satellite peaks consistent with the clock distortions [19]; the observation of these peak splitting signatures has been made possible by improved experimental resolution since the time of the original studies. In addition, the versatility of the resonant scattering method has been expanded in recent years; for example, superlattice signatures of SmC* variant phases have now been observed for compounds containing either bromine or selenium atoms; by working at the higher energy Br [20] or Se [21] absorption edges (13.49 KeV and 12.66 KeV, respectively), the need to work in a helium atmosphere is relaxed. For example, resonant scattering superlattice signatures have been obtained from Se-containing liquid crystals in bulk liquid-crystal cell geometries [21]; these results demonstrate that resonant scattering can also be a powerful tool for revealing structural information directly relevant to the application of SmC* variant phases in displays and optical switching devices.

References

[1] Chandani, A. D. L., Gorecka, E., Ouchi, Y., Takezoe, H., and Fukuda, A., 1989, *Jpn. J. Appl. Phys.*, **28,** L1265.

[2] Fukuda, A., Takanishi, Y., Isozaki, T., Ishikawa, K., and Takezoe, H., 1994, *J. Mater. Chem.*, **4,** 997.

[3] Itoh, K., Kabe, M., Miyachi, K., Takanishi, Y., Ishikawa, K., Takezoe, H., and Fukuda, A., *J. Mater. Chem.*, **7,** 407.

[4] Hiraoka, K., Tsumita, T., Sugiyama, Y., Monzen, K., Uematsu, Y., and Suzuki, Y., 1997, *Jpn. J. Appl. Phys.*, **36,** 6847.

[5] Gorecka, E., Chandani, A. D. L., Ouchi, Y., Takezoe, H., and Fukuda, A., 1990, *Jpn. J. Appl. Phys.*, **29,** 131.

[6] Galerne, Y., and Liebert, L., 1991, *Phys. Rev. Lett.*, **66,** 2891.

[7] Bahr, Ch., and Fliegner, D., 1993, *Phys. Rev. Lett.*, **70,** 1842.

[8] Takanishi, Y., Ikeda, A., Takezoe, H., and Fukuda, A., 1995, *Phys. Rev. E*, **51,** 400.

[9] Dmitrienko, V. E., 1983, *Acta Cryst.*, **A39,** 29.

[10] Levelut, A.-M., and Pansu, B., 1999, *Phys. Rev. E*, **60,** 6803.

[11] Cepic, M., and Zeks, B., 1995, *Mol. Cryst. Liq. Cryst.*, **263,** 61; Lorman, V. L., 1995, *Mol. Cryst. Liq. Cryst.*, **262,** 437; Pikin, S. A., Hiller, S., and Haase, W., 1995, *Mol. Cryst. Liq. Cryst.*, **262,** 425; Roy, A., and Madhusudana, N., 1996, *Europhys. Lett.*, **36,** 221.

[12] We use the maximum of the fluorescence intensity to define the sulphur K-edge energy for the purposes of our studies.

[13] Mach, P., Pindak, R., Levelut, A.-M., Barois, P., Nguyen, H. T., Huang, C. C., and Furenlid, L., 1998, *Phys. Rev. Lett.*, **81,** 1015.

[14] Isozaki, T., Fujikawa, T., Takezoe, H., Fukuda, A., Hagiwara, T., Suzuki, Y., and Kawamura, I., 1992, *Jpn. J. Appl. Phys.*, **31,** L1435; Hiraoka, K., Takanishi, Y., Sharp, K., Takezoe, H., and Fukuda, A., 1991, *Jpn. J. Appl. Phys.*, **30,** L1819.

[15] Mach, P., Pindak, R., Levelut, A.-M., Barois, P., Nguyen, H. T., Baltes, H., Hird, M., Toyne, K., Seed, A., Goodby, J., Huang, C. C., and Furenlid, L., 1999, *Phys. Rev. E*, **60,** 6793.

[16] Johnson, P. M., Pankratz, S., Mach, P., Nguyen, H. T., and Huang, C. C., 1999, *Phys. Rev. Lett.*, **83,** 4073.

[17] Akizuki, T., Miyachi, K., Takanishi, Y., Ishikawa, K., Takezoe, H., and Fukuda, A., 1999, *Jpn. J. Appl. Phys.*, **38,** 4832.

[18] Johnson, P. M., Olson, D. A., Pankratz, S., Nguyen, T., Goodby, J., Hird, M., and Huang, C. C., 2000, *Phys. Rev. Lett.*, **84,** 4870.

[19] Cady, A., Pitney, J. A., Pindak, R., Matkin, L. S., Watson, S. J., Gleeson, H. F., Cluzeau, P., Barois, P., Levelut, A.-M., Caliebe, W., Goodby, J. W., Hird, M., and Huang, C. C., 2001, *Phys. Rev. E*, **64,** 50702(R).

[20] Cluzeau, P., Gisse, P., Ravaine, V., Levelut, A.-M., Barois, P., Huang, C. C., Rieutord, F., and Nguyen, H. T., 2000, *Ferroelectrics*, **244,** 301.

[21] Matkin, L. S., Gleeson, H. F., Mach, P., Huang, C. C., Pindak, R., Srajer, G., Pollmann, J., Goodby, J. W., Hird, M., and Seed, A., 2000, *Appl. Phys. Lett.*, **76,** 1863.